Enhanced stability of Ni/SiO_2 catalyst for CO_2 methanation: Derived from nickel phyllosilicate with strong metal–support interactions

Run-Ping Ye [a, b, c, 1], Weibo Gong [a, 1], Zhao Sun [a], Qingtao Sheng [a, d], Xiufeng Shi [a, d], Tongtong Wang [a], Yi Yao [a], Joshua J. Razink [e], Ling Lin [b], Zhangfeng Zhou [b], Hertanto Adidharma [a], Jinke Tang [f], Maohong Fan [a, g, h, i, *], Yuan-Gen Yao [b, **]

[a] Department of Chemical Engineering, University of Wyoming, Laramie, WY, 82071, USA
[b] Key Laboratory of Coal to Ethylene Glycol and Its Related Technology, Fujian Institute of Research on the Structure of Matter, Chinese Academy of Sciences, Fuzhou, Fujian, 350002, PR China
[c] University of Chinese Academy of Sciences, Beijing, 100049, PR China
[d] Institute of Special Chemicals, Taiyuan University of Technology, Taiyuan, 030024, PR China
[e] Center for Advanced Materials Characterization in Oregon, University of Oregon, Eugene, OR, 97403, United States
[f] Departments of Physics & Astronomy, University of Wyoming, Laramie, WY, 82071, USA
[g] Department of Petroleum Engineering, University of Wyoming, Laramie, WY, 82071, USA
[h] School of Energy Resources, University of Wyoming, Laramie, WY, 82071, USA
[i] School of Civil and Environmental Engineering, Georgia Institute of Technology, Atlanta, GA, 30332, USA

A B S T R A C T

Nowadays more and more significant technologies have been developing to save energy and reduce emissions. CO_2 methanation has been an attractive process to reduce CO_2-emissions since it consumes CO_2 with H_2 derived from renewable energy sources to produce CH_4. However, the poor stability of Ni-based catalyst for CO_2 methanation is still challenging. Herein, two Ni/SiO_2 catalysts with different structure and catalytic properties were prepared by different methods. The Ni/SiO_2-AEM nanocatalyst with a lamellar structure of nickel phyllosilicate was synthesized by a facile ammonia-evaporation method (AEM), which can conveniently and uniformly disperse nickel species on SiO_2. Upon reduction of nickel phyllosilicate, it can disperse and confine small sized Ni particles (4.2 nm) in the silica support with a high surface area of 446.3 m^2/g, leading to the Ni/SiO_2-AEM catalyst achieving a high yield of methane with long-term stability of 100 h under the GHSV of 10,000 mL/(g_{cat} h) and another 60 h with the GHSV increased to 30,000 mL/(g_{cat} h) at 370 °C. In comparison, the Ni/SiO_2-IM catalyst prepared by the impregnation method obtained lower yield of methane and worse stability under identical conditions. The results indicate that the catalyst with high surface area and strong metal-support interactions can improve stability.

© 2019 Published by Elsevier Ltd.

1. Introduction

The catalytic conversion of carbon dioxide (CO_2) has not only provided an alternative way to reuse the fossil-carbon resource and close the anthropogenic carbon cycle, but also synthesized high-value chemicals and fuels. Considerable work has focused on the CO_2 methanation reaction because it is a thermodynamically favourable reaction in C1 chemistry ($\Delta G_{298K} = -130.8$ kJ/mol) [1], which can convert CO_2 with H_2 derived from renewable energy sources to valuable methane (CH_4) under relatively mild conditions with high energy efficiency [2]. Therefore, developing new catalysts associated with CO_2-utilization through green processes is beneficial for mitigating energy and environment issues. Methane, a principal component of natural gas, can either be directly used as a fuel or in other applications such as reforming with CO_2 to produce syngas [3].

The catalysts for CO_2 methanation have been intensively

Nomenclature		BET	Brunauer-Emmett-Teller
		NiPS	Nickel phyllosilicate
AEM	Ammonia-evaporation method	NiO	Nickel oxide
IM	Impregnation method	SiO_2	Silicon dioxide
ΔG	Gibbs free energy	H_2	Hydrogen
S_{BET}	Specific surface area	CH_4	Methane
V_p	Pore volume	CO_2	Carbon dioxide
GHSV	Gas hourly space velocity	CO	Carbon monoxide
SEM	Scanning electron microscopy	X_{CO2}	CO_2 conversion
EDS	Energy dispersive spectroscopy	S_{CH4}	CH_4 selectivity
TEM	Transmission electron microscopy	Y_{CH4}	CH_4 yield
XRD	Powder X-ray diffraction	ICP-OES	Inductively coupled plasma optical emission
XPS	X-ray photoelectron spectroscopy		spectrometry
DRIFTS	Diffuse Reflectance Infrared Fourier Transform	TCD	Thermal conductivity detector
	Spectroscopy	GC	Gas chromatograph
IR	Infrared spectra	NH_3-TPD	Ammonia temperature-programmed desorption
H_2-TPR	Hydrogen temperature-programmed reduction		

investigated so far. Among them, the noble metals (Ru, Rh, Pd)-based catalysts have been well developed due to their high activity and long-term stability, but their large scale application is limited [4]. Also, the Ni-based catalysts are much preferred because of their excellent catalytic performance and a low price compared to the noble metals. However, the Ni-based catalysts often suffer the problem of poor stability from carbon deposition, sintering, and chemical poisoning [5]. In particular, the Ni/SiO_2 catalysts prepared by impregnation method (IM) would be deactivated in 20 h (10%Ni/SiO_2-IM [6], 20%Ni/SiO_2-IM [7]). Therefore, the biggest challenge for CO_2 methanation over Ni-based catalysts is their poor stability. Numerous efforts have been taken to develop stable Ni-based catalysts. The state of the art is as following: Firstly, doping the Ni catalysts with a second metal to form alloy can result in changing the surface morphology with more small and well-defined NPs [8]. The Ni-Mg [6], Ni-Fe [9], Ni—Ru, Ni-Pd [10], and rare earth (La, Ce, Sm, and Pr) [11] doped Ni systems were reported to enhance the activity and stability. Secondly, modifying the supports has been another strategy to improve the stability [12]. A series of supports such as SiO_2 [7], SBA-15/16 [13], MCM-41 [14], TiO_2 [15], Al_2O_3 [16], ZrO_2 [17], CeO_2 [18] and MOFs [19] have been used to prepare stable Ni-based catalysts for CO_2 methanation from the perspective of improving the metal-support interactions. Thirdly, it is suggested to design the Ni-based catalysts with special structures like hydrotalcites and perovskites, which possess higher thermal stability against sintering [20]. Fourthly, altering preparation methods is another solution to dealing with the deactivation problem [21]. The impregnation method (IM) is convenient to synthesize catalysts in a large scale, but the prepared catalysts often exhibit weak metal-support interactions and low metal dispersion, especially under the condition of high metal loading. Hence, more methods are needed to prepare high-performance and long-lived Ni-based catalysts. For example, a microwave-assisted method was used to obtain more Ni active sites and higher nickel dispersed 20%Ni/Al_2O_3-Mm catalyst than the comparative 20%Ni/Al_2O_3-Im catalyst prepared by IM [22]. The 20%Ni/Al_2O_3-M catalyst exhibited a good stability of 72 h for CO_2 methanation.

The preparation methods play significant roles in regulating the catalyst's morphology and influencing the metal-support interactions. Thus, this work is aimed to improve the stability of Ni/SiO_2 catalyst for CO_2 methanation via enhancing metal-support interactions to suppress nickel sintering, which can be achieved by designing a different preparation method, namely ammonia-evaporation method (AEM). Different from impregnation method,

the AEM needs to use ammonia aqueous solution and colloidal silica, which can conveniently and uniformly disperse metal species on SiO_2 during ammonia evaporation process. The experimental operation and condition is also facile and mild. Therefore, the AEM has been widely used to prepare stable Cu-based catalysts for the hydrogenation of dimethyl oxalate [23], methyl acetate [24], ethylene carbonate [25], furfural [26], and CO_2 [27] to alcohols. The reason is that Cu-based catalysts prepared by AEM can produce copper phyllosilicate, which can lead to larger surface area, higher metal dispersion, and stronger metal-support interactions [27]. However, the Ni-based catalysts prepared by the AEM have been reported on less frequently than Cu-based catalysts. In fact, the Ni—Si based catalysts with rod-like nickel phyllosilicate (NiPS) prepared by AEM exhibit outstanding stability in many high-temperature reactions. After a Ni/SiO_2-AEM catalyst was reported to possess good stability for steam reforming of ethanol [28], Zhang et al. studied a stable Ni/SBA-15 catalyst for dry reforming of CH_4 [29]. Additionally, Yang et al. prepared a series of Ni/SiO_2 catalysts with different nickel loading via modified AEM for deoxygenation of m-cresol to toluene [30]. Although the AME prepared Ni-based catalysts have been studied for several different processes, until now, a detailed study on Ni/SiO_2 catalysts prepared by AEM for CO_2 methanation process has not yet to be published. Therefore, the novelty of this work is to enhance the stability of Ni/SiO_2 catalyst with unique layered structure for CO_2 methanation prepared by a facile method without using any promoter or noble metal.

In the present work, the Ni/SiO_2-AEM catalyst prepared by the ammonia-evaporation method was chosen as a modelling approach to improve the catalytic stability for CO_2 methanation. The NiPS was achieved in this catalyst, resulting in a high yield of methane with long-term stability up to 160 h. A Ni/SiO_2-IM catalyst was also synthesized for comparison by impregnation method. A variety of characterization techniques such as XRD, TEM and TPR were used to reveal the reason for the ammonia-evaporation method being a more suitable route than the impregnation method to prepare excellent Ni/SiO_2 catalysts for CO_2 methanation.

2. Experiment

2.1. Catalyst preparation

The Ni/SiO_2 with a theoretical nickel loading of 40.0 wt% was synthesized by the ammonia-evaporation method. All the materials were obtained and used from commercial sources. Briefly, 11.632 g

of nickel nitrate hexahydrate (*Sigma-Aldrich, CAS: 13,478-00-7*) was dissolved in 150 mL of DI water (pH = 4.82). Then 25 mL of 28.0−30.0 wt% ammonium hydroxide solution (*Sigma-Aldrich, CAS: 1336-21-6*) and 11.8 g of 30.0 wt% LUDOX®AS-30 (*Sigma-Aldrich, CAS: 7631-86-9*) colloidal silica were added (pH = 11.32) and stirred for 5 h at room temperature (pH = 10.72). The suspension was vigorously stirred at 80 °C in a water bath to allow for the evaporation of ammonia until the pH value decreased to 6−7 (pH = 6.72), and the color of the suspension was changed simultaneously from blue to green. The light green precipitate was obtained by filtering and washing with DI water. The catalyst precursor was dried at 80 °C for 12 h before calcined at 450 °C for 4 h in air. The obtained sample was denoted as Ni/SiO$_2$-AEM catalyst.

For comparison, another Ni/SiO$_2$ with the same nickel loading of 40.0 wt% was prepared by the impregnation method. Namely, 11.632 g of nickel nitrate hexahydrate (*Sigma-Aldrich, CAS: 112,926-00-8*) was dissolved in 150 mL of DI water. Then 3.54 g of silica gel (*Sigma-Aldrich, high-purity grade, 200−400 mesh particle size*) was added and vigorously stirred at 70 °C in a water bath until water was evaporated. The catalyst precursor was dried at 90 °C for 12 h and then calcined at 450 °C for 4 h in air. The obtained sample was denoted as Ni/SiO$_2$-IM catalyst. The schematic of the catalyst preparation is shown in Fig. 1.

2.2. Catalyst characterization

N$_2$ adsorption-desorption isotherms were obtained by an *automatic Quantachrome instrument* using N$_2$ physisorption at 77 K. The samples (about 110 mg) were evacuated at 250 °C for 3 h prior to the N$_2$ physisorption measurement. The Brunauer-Emmett-Teller (BET) method was used to determine the specific surface area (S$_{BET}$) of the catalyst. The infrared (IR) spectra were collected on a *Nicolet iS5*0 ATR *spectrometer* with a spectral resolution of 4 cm^{-1}. The *in-situ* DRIFTS spectra were collected using a *Nicolet 6700 spectrometer*. The X-ray diffraction (XRD) analysis was conducted on a *Rigaku Smartlab diffractometer* with a Cu Kα radiation source under 40 kV and 40 mA. The 2θ range was from 10° to 85° with a scanning speed of 5°/min. Scanning electron microscopy (SEM) and energy dispersive spectroscopy (EDS) were performed on a *FEI Quanta FEG 450 apparatus* with an acceleration voltage of 20 kV. Transmission electron microscopy (TEM) was performed on *a FEI 80−300 Titan (S)TEM* equipped with a spherical aberration image corrector at 300 kV. TEM samples were prepared by sonicating the catalysts in ethanol and then drop casting the suspension on a TEM grid. Hydrogen temperature-programmed reduction (H$_2$-TPR) and ammonia temperature-programmed desorption (NH$_3$-TPD) tests were performed on *Autosorb IQ quantachrome instrument* (ASI-QAC160000-6 for H$_2$-TPR and ASIQC0100-4 for NH$_3$-TPD), equipped with thermal conductivity detector (TCD). For the H$_2$-TPR, after treated at 160 °C for 0.5 h in He (US Welding), the sample (about 100 mg) was cooled and then heated to 930 °C at 10 °C/min under the gas of 5 vol% H$_2$-95 vol% N$_2$ (5.0 UHP). For the NH$_3$-TPD test, the sample (about 100 mg) was pretreated at 250 °C for 1 h in He. Then the sample was reduced at 500 °C for 3 h in 5 vol% H$_2$-95 vol% N$_2$. The sample was cooled down to 50 °C and a flow of 10 vol% NH$_3$-90 vol% N$_2$ (5.0 UHP) gas mixture was fed through the sample for 1 h. The residual NH$_3$ was blown off under the He flow for another 1 h. At last the NH$_3$-TPD test was carried out from 50 to 930 °C at a heating rate of 10 °C/min under He flow. The X-ray photoelectron spectroscopy (XPS) spectra were taken on a ThermoScientifc ESCALAB 250 instrument with monochromatized Al X-ray source at the University of Oregon. The binding energy scales were calibrated with the C1s (284.8 eV). The actual Ni contents on the prepared catalysts were determined by inductively coupled plasma optical emission spectrometry (ICP-OES) analysis in a *Jobin Yvon Ultima2*.

2.3. Catalyst evaluation

The CO$_2$ methanation reaction was performed in a fixed-bed set-up with a reaction tube (i.d. 10 mm, length 610 mm). 300 mg of catalyst with 500 mg of silica sand were mixed and sandwiched by quartz wool in the middle of the tube. Silica sand was not used in the long-term stability test. Then the sample was *in-situ* reduced in a pure H$_2$ stream (5.0 UHP, 30 mL/min) at 500 °C for 2 h under the
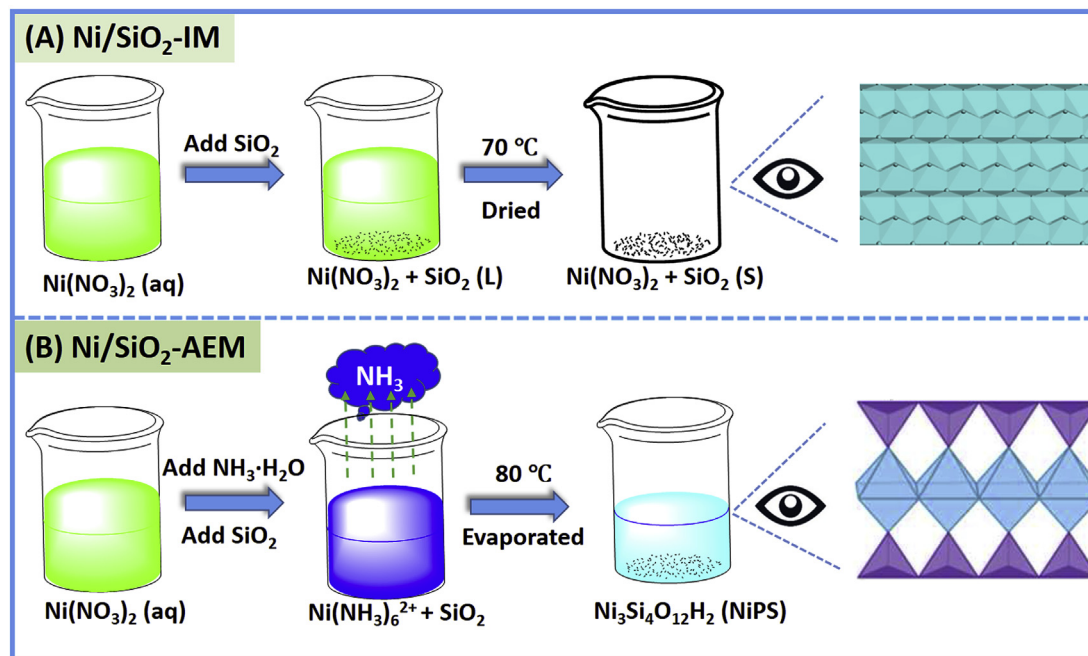

Fig. 1. The schematic of two Ni/SiO$_2$ catalysts prepared by the impregnation method (IM) and ammonia-evaporation method (AEM).

pressure of 1.0 MPa. The Ni/SiO$_2$-AEM sample reduced at 800 °C for 2 h in the tube furnace was labeled as Ni/SiO$_2$-AEM (800 °C). After the reduction, the temperature was cooled down to the reaction temperature (290−470 °C) and the pressure was decreased to atmospheric pressure (about 0.1 MPa). A mixture of H$_2$ and CO$_2$ (4.0 IS) with a molar ratio of 4:1 was introduced into the reactor with a gas hourly space velocity (GHSV) of 10,000 or 30,000 mL/(g$_{cat}$ h). For the stability test, 300 mg of the Ni/SiO$_2$ catalyst with 500 mg of silica was reduced at 500 °C for 2 h under the pressure of 1.0 MPa. The catalyst stability was first evaluated under a GHSV of 10,000 mL/(g$_{cat}$ h) at 370 °C and 0.1 MPa for time-on-stream of 100 h, and then the GHSV was increased to 30,000 mL/(g$_{cat}$ h) for another 60 h without changing other conditions. The outlet gas was analyzed by an on-line gas chromatograph (GC, SRI 8610C) equipped with a Porapak Q column and a TCD. The CO$_2$ conversion (X_{CO2}), CH$_4$ selectivity (S_{CH4}) and CH$_4$ yield (Y_{CH4}) were calculated using the equations as follows, where $M_{in\ or\ out}$ is the moles of inlet gas and outlet gas, respectively; $P_{CO2,\ in}$ is the mole ratio of CO$_2$ in inlet gas and $P_{CO2/CH4,\ out}$ is the mole ratio of CO$_2$/CH$_4$ in outlet gas.

$$X_{CO2}(\%) = \frac{M_{in}*P_{CO2,in} - M_{out}*P_{CO2,out}}{M_{in}*P_{CO2,in}} \times 100\%$$

$$S_{CH4}(\%) = \frac{M_{out}*P_{CH4,out}}{M_{in}*P_{CO2,in} - M_{out}*P_{CO2,out}} \times 100\%$$

$$Y_{CH4}(\%) = X_{CO2}(\%) \times S_{CH4}(\%) \times 100\%$$

3. Results and discussions

3.1. N$_2$ adsorption-desorption analysis

Fig. 2 shows the type IV nitrogen adsorption-desorption isotherms of the two Ni/SiO$_2$ catalysts prepared by AEM and IM methods. Two major differences should be noted. One is that the Ni/SiO$_2$-AEM exhibits higher nitrogen adsorption-desorption isotherms than the Ni/SiO$_2$-IM, indicating that the former has larger specific surface area and pore volume (S$_{BET}$: 446.3 vs. 307.2 m^2/g; V$_p$: 0.84 vs. 0.45 cm^3/g). This is rationalized by the formation of layered structures in the sample prepared by ammonia-evaporation method [31]. The other difference is that the hysteresis loop for the sample prepared by IM is a typical H1 type while the shape of the hysteresis loop for Ni/SiO$_2$-AEM is a typical H3 type at P/P$_0$ of 0.4−1.0, owing to the presence of slit-shaped mesopores and channels [32].

3.2. XRD and IR analyses

Fig. 3 presents XRD patterns of the Ni/SiO$_2$ samples. Five characteristic diffraction peaks at 26.7°, 33.7°, 39.7°, 53.2° and 60.9° over the calcined Ni/SiO$_2$-AEM are assigned to NiPS in Fig. 3A (PDF#43−0664) [31]. However, the calcined Ni/SiO$_2$-IM shows five sharp diffraction peaks of NiO (PDF#44−1159) [33], indicating the existence of bulk NiO nanoparticles. Upon reduction at 500 °C, the Ni/SiO$_2$-IM possesses obvious diffraction peaks of Ni^0 (PDF#04−0850) [33], which are not present in the Ni/SiO$_2$-AEM, indicating well-dispersed Ni species in the Ni/SiO$_2$-AEM (Fig. 3B). However, the diffraction peaks of Ni^0 are shown in the Ni/SiO$_2$-AEM (800 °C) due to some Ni species sintering upon reduction at 800 °C. In addition, the reduced Ni/SiO$_2$-AEM also shows some weak diffraction peaks of NiO. It is probably because the NiPS was partially destroyed and decomposed to NiO after reduction. The
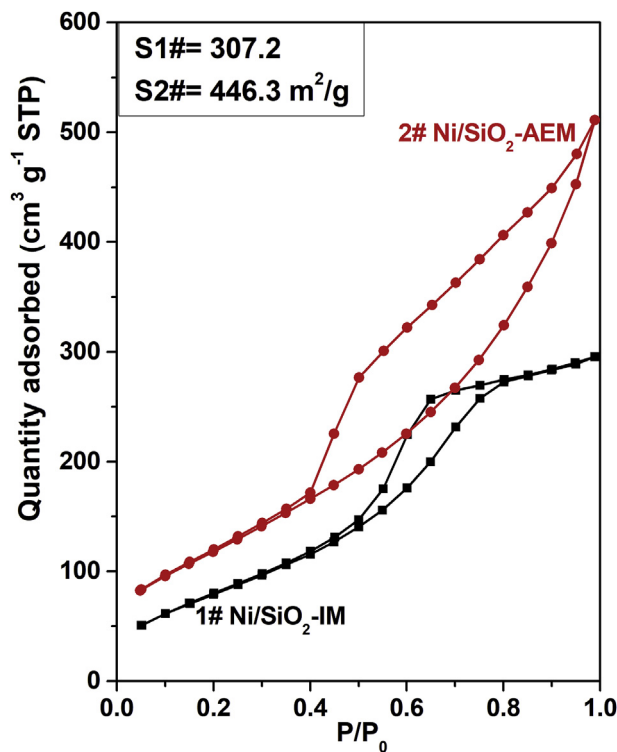

Fig. 2. Nitrogen adsorption-desorption isotherms of Ni/SiO$_2$ samples.

small and fine dispersion of Ni^0 may also be oxidized during the test process.

The IR spectra were used to further determine the existence of NiPS. As shown in Fig. 4A, the band at 1115/1051 cm^{-1} and 800 cm^{-1} are ascribed to the υ$_{SiO}$ asymmetric and symmetric stretching band of silica support, respectively [34]. The formation of NiPS is illustrated by the presence of the δ$_{OH}$ band at 674 cm^{-1} and the υ$_{SiO}$ shoulder peak at 1023 cm^{-1} in the calcined Ni/SiO$_2$-AEM while not present in the Ni/SiO$_2$-IM [35]. After reduction treatment, the intensities of the bands at around 670 and 1045 cm^{-1} decreased for 500 °C reduced Ni/SiO$_2$-AEM while they disappeared for the 800 °C reduced sample (Fig. 4B). The results suggest that some of the NiPS is still present after reduction at 500 °C, while it is completely destroyed after reduction at 800 °C.

3.3. Morphology analysis

The SEM images of the calcined samples are shown in Fig. 5. As can be seen, the silica particles in the Ni/SiO$_2$-IM are much larger (Fig. 5A vs. Fig. 5B). In addition, the spherical-like shape particles in the Ni/SiO$_2$-AEM are smaller and uniformly distributed, thus the Ni, O, and Si element distributions are well-dispersed in the EDS mapping (Fig. 5D−F).

Fig. 6 illustrates the TEM images of Ni/SiO$_2$ catalysts. As proved with the XRD and SEM results above, the calcined Ni/SiO$_2$-IM displays large NiO particles in Fig. 6A. The rod-like NiPS is shown in the calcined Ni/SiO$_2$-AEM, indicating the formation of the layered structures of NiPS (Fig. 6C). After reduction treatment, the rod-like morphology of NiPS nearly disappeared, whereas small black spherical particles were assigned to metallic nickel (Fig. 6G and H). Furthermore, the mean particle size of the reduced Ni/SiO$_2$-AEM at 500 °C is about 4.2 nm, which is calculated using the *Nano Measurer 1.2* software. Ni^0 particles in the Ni/SiO$_2$-AEM reduced at 800 °C have an obviously larger particle size (~6.0 nm) than the Ni/SiO$_2$-
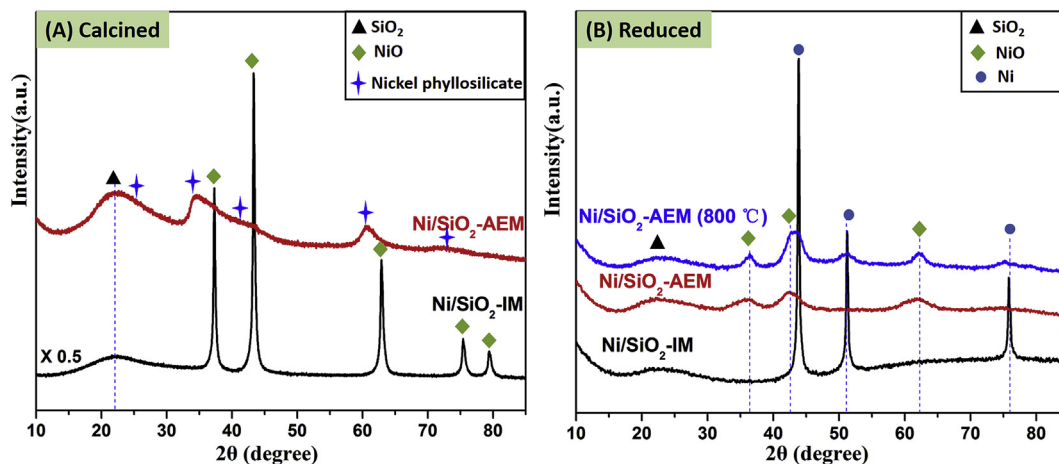
Fig. 3. XRD patterns of the Ni/SiO$_2$ samples.
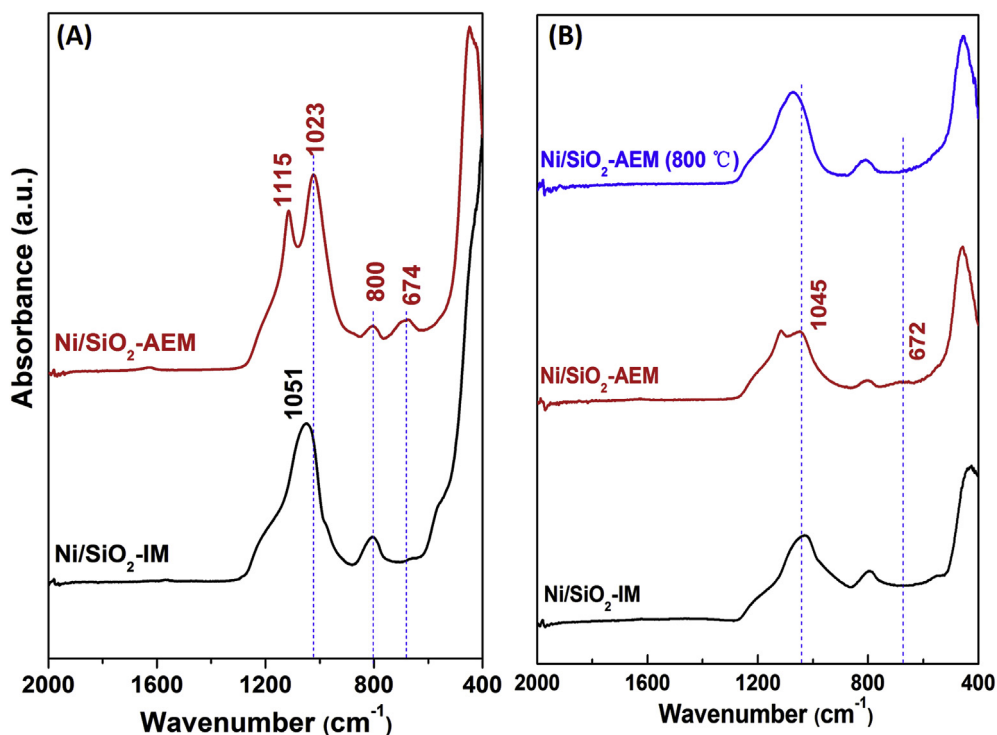
Fig. 4. IR spectra of calcined (A) and reduced (B) Ni/SiO$_2$ samples.

AEM reduced at 500 °C, but still smaller than those in the reduced Ni/SiO$_2$-IM (~12.0 nm). Therefore, the high dispersion of nickel particles suggests a strong Ni–Si interaction in the Ni/SiO$_2$-AEM.

3.4. H$_2$-TPR and NH$_3$-TPD analyses

Since the above-mentioned nickel phyllosilicate (NiPS) exists in the structure of Ni/SiO$_2$-AEM, one has to ask if the NiPS will affect the reducibility and surface acid properties of the catalysts. As shown in Fig. 7A, the Ni/SiO$_2$-IM shows a strong reduction peak at 388 °C and a weak shoulder peak at around 510 °C, which can be assigned to the reduction of nickel oxide and the isolated nickel ions (+2) that interact weakly with the silica, respectively. However, for the Ni/SiO$_2$-AEM, only a relatively broad reduction peak at

400–800 °C, owing to the more difficult reduction of Ni^{2+} located in NiPS with a strong metal-support interaction [36]. Similarly, the Ni/SiO$_2$-IM shows a small number of acid sites while the Ni/SiO$_2$-AEM has much larger amount of weak, middle, and strong acid sites (Fig. 7B). The acid sites in the Ni/SiO$_2$-AEM come from the unsaturated Ni^{2+} and surface OH sites on the NiPS structure [31]. Therefore, the nickel species of NiPS significantly enhance the interactions between Ni^{2+} and SiO$_2$, as well as increasing the amount of surface acid sites over the Ni/SiO$_2$-AEM.

3.5. XPS analysis

The chemical states of nickel species in the Ni/SiO$_2$ catalysts before and after reduction were characterized by XPS. As illustrated
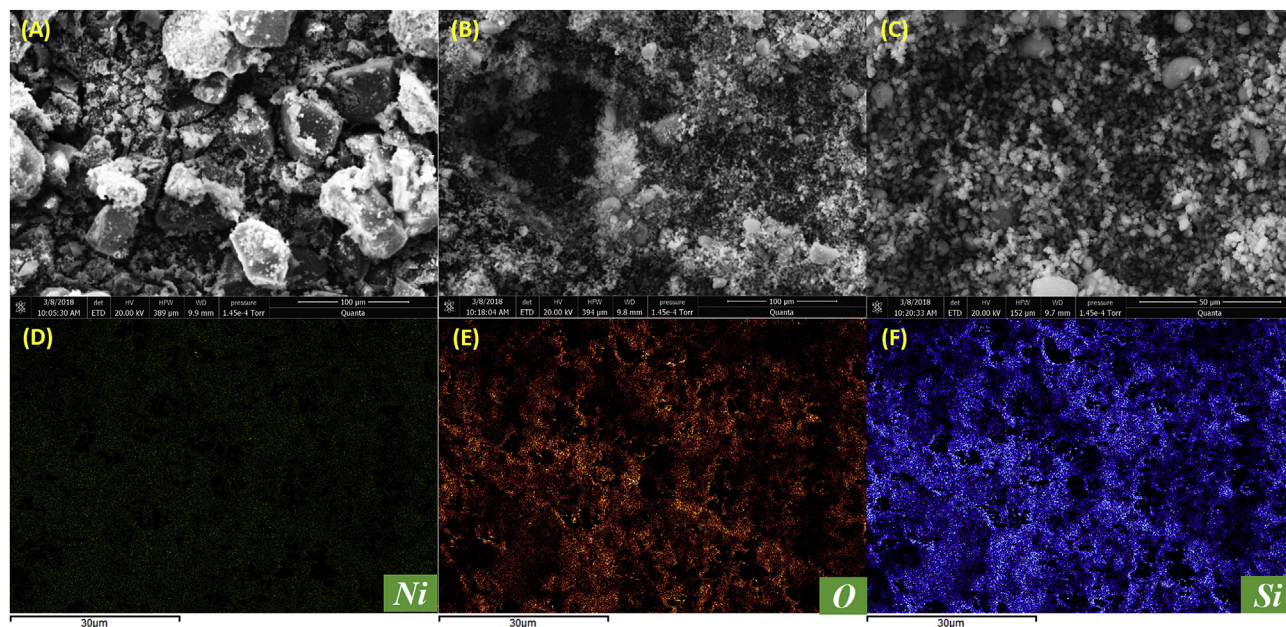
Fig. 5. SEM images of the calcined Ni/SiO$_2$-IM (A) and Ni/SiO$_2$-AEM (B, C), and EDS mapping of Ni/SiO$_2$-AEM (D–F).
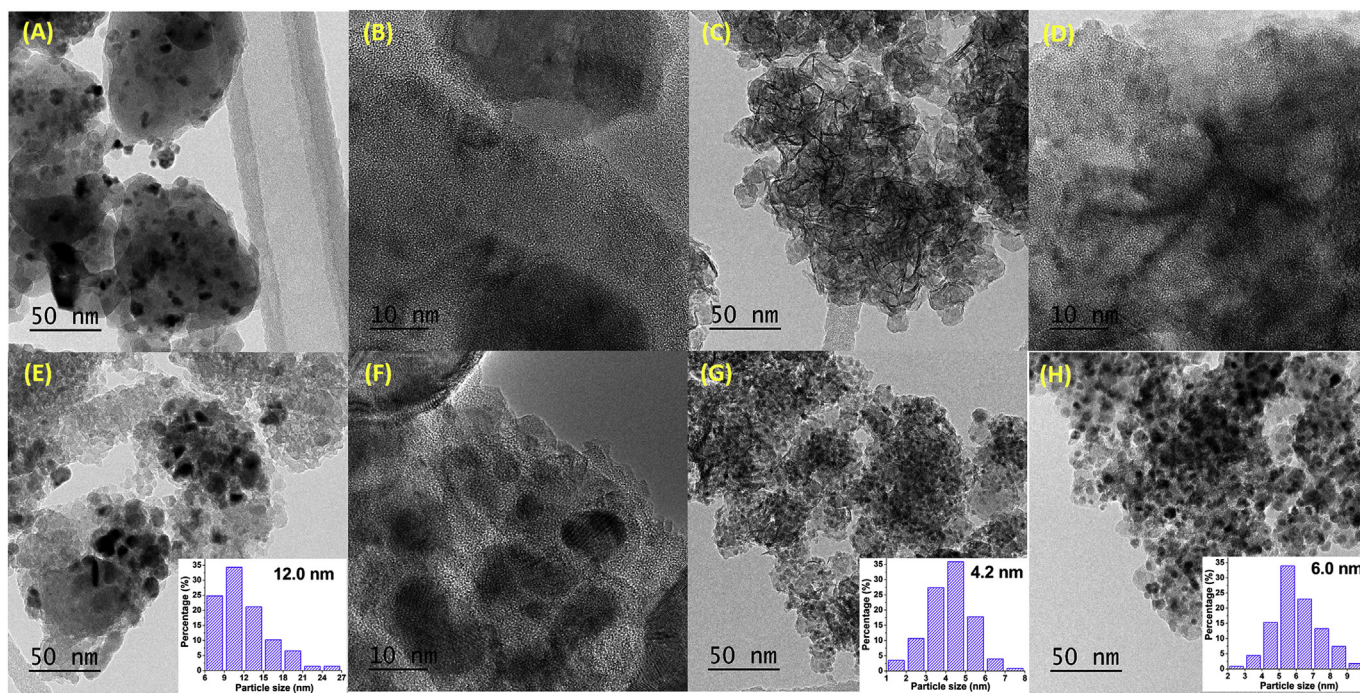
Fig. 6. TEM images of the calcined Ni/SiO$_2$-IM (A, B), calcined Ni/SiO$_2$-AEM (C, D), reduced Ni/SiO$_2$-IM (E, F), Ni/SiO$_2$-AEM reduced at 500 °C (G), and Ni/SiO$_2$-AEM reduced at 800 °C (H). Insets are the Ni size distribution.

in Fig. 8, the results can infer several following aspects: (1) the content of surface nickel species over the Ni/SiO$_2$-AEM is higher than those in the Ni/SiO$_2$-IM, as the former peak's intensity is stronger and the atomic percentages of Ni in the reduced samples are 13.1% and 8.3%, respectively. However, the ICP-OES results indicated that the actual Ni loading in the reduced Ni/SiO$_2$-IM and Ni/SiO$_2$-AEM catalysts were 39.58% and 25.73%, respectively. The lower Ni loading over Ni/SiO$_2$-AEM is probably because that some nickel ions weakly absorbed on silica gel were eluted during

filtering and washing process. (2) The nickel species in the calcined Ni/SiO$_2$ are different. The Ni/SiO$_2$-AEM-Calcined sample exhibits only one Ni2p$_{3/2}$ peak at 858.8 eV, which is assigned to NiPS [37]. However, for the Ni/SiO$_2$-IM-Calcined sample, it exhibits two Ni2p$_{3/2}$ peaks at 856.2 and 854.2 eV, which are attributed to highly dispersed NiO and aggregated NiO, respectively [38]. (3) After reduction, there are still many Ni^{2+} in the Ni/SiO$_2$-AEM-Reduced sample while Ni^0 in the Ni/SiO$_2$-IM-Reduced sample.
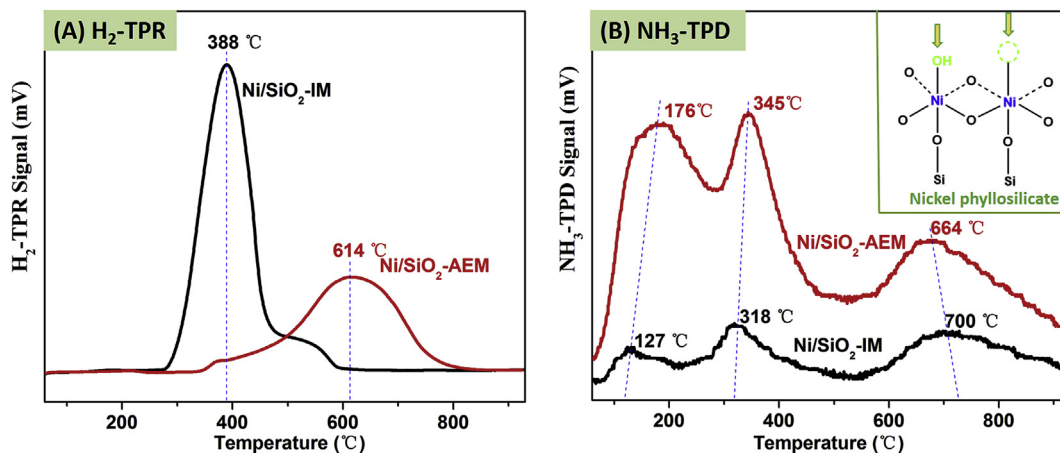
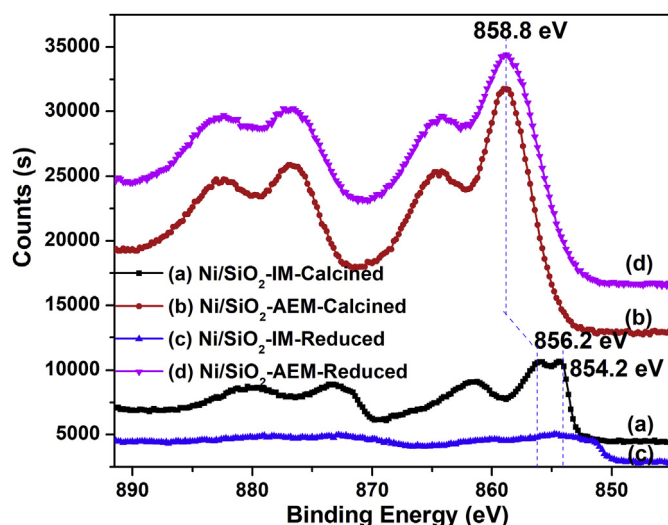**Fig. 7.** The temperature programmed profiles of Ni/SiO$_2$ catalysts.

Fig. 8. Ni2p XPS spectra of the Ni/SiO$_2$ catalysts before and after reduction.

3.6. Catalytic performance

The CO$_2$ methanation was performed in the temperature range of 290−470 °C with GHSV of 10,000 mL/(g$_{cat}$ h) at the pressure of 0.1 MPa, with the results being shown in Fig. 9. The dashed lines in Fig. 9A−C represent the thermodynamic equilibrium [39]. Firstly, the Ni/SiO$_2$-AEM samples show better catalytic activities than the Ni/SiO$_2$-IM, but still slightly lower than equilibrium value. Secondly, the catalytic performance of the Ni/SiO$_2$-AEM reduced at different temperatures (500 and 800 °C) are very similar in the 370−470 °C temperature range, indicating that partially reduced NiPS would not seriously influence the activity. In addition, the Y_{CH4} of the Ni/SiO$_2$-AEM is 75.52% at 370 °C, which is higher than 55.94% for the Ni/SiO$_2$-IM (Fig. 9C).

To further evaluate the stability of the catalysts, the stability test of 100 h was carried out at 10,000 mL/(g$_{cat}$ h) and another 60 h lifetime test at 30,000 mL/(g$_{cat}$ h) under the optimal reaction temperature of 370 °C was also performed. As shown in Fig. 9D−F, the activity of Ni/SiO$_2$-AEM remains high and stable over the lifetime test. When the GHSV is increased threefold, both the CO$_2$ conversion and CH$_4$ yield decrease for the catalysts. Moreover, the Y_{CH4} of the Ni/SiO$_2$-IM slightly decreased in the last 20 h on stream under the high GHSV, indicating its slightly deactivation. The TEM

images and XRD results of the spent Ni/SiO$_2$ samples are presented in Figs. S1−S2, which clearly confirms that the presence of NiPS in the spent Ni/SiO$_2$-AEM again. Fortunately, the average Ni particle size of the spent Ni/SiO$_2$-AEM is still 5.2 nm, which are not much larger than those in the reduced catalyst (4.2 nm). In addition, the used Ni/SiO$_2$-IM also displays some weak diffraction peaks corresponding to NiO (Fig. S2), which are not seen in the freshly reduced Ni/SiO$_2$-IM (Fig. 3). The sintering of Ni particles during the stability test is more obvious for the Ni/SiO$_2$-IM (Fig. 6E, F vs. Fig. S1A, B, 12.0 nm vs. 15.0 nm). Therefore, the Ni/SiO$_2$-AEM exhibits a higher activity and better stability compared to the Ni/SiO$_2$-IM.

3.7. Structure-performance relationship

It is worth noting that the evolution of NiPS has played significant roles in the structure of the catalyst and the CO$_2$ methanation reaction. Several characterization methods, including XRD (Fig. 3), IR (Fig. 4), TEM (Fig. 6), H$_2$-TPR and NH$_3$-TPD (Fig. 7) and XPS (Fig. 8) are used to prove the formation of NiPS in the calcined Ni/SiO$_2$-AEM precursor. The lamellar structure of NiPS has the advantages of larger S$_{BET}$, more surface acid sites, and anchoring the Ni particles in the channels. Upon reduction at 500 °C, the crystallinity of NiPS is mostly destroyed, but some is still reserved, as evidenced by the XRD and IR results in Figs. 3 and 4. The XRD (Fig. 3B) and H$_2$-TPR (Fig. 7) results illustrate that the NiPS can be completely reduced under the temperature higher than 800 °C. However, larger particle size of nickel species is obtained when reduced at 800 °C as shown in the TEM image (Fig. 6H). Furthermore, the catalytic performance of the Ni/SiO$_2$-AEM reduced at 500 °C is not affected when the reaction temperature is further increased to higher than 370 °C (Fig. 9). After the long-term stability test, some nickel species were oxidized to NiPS again (Figs. S1−S2). In our previous work [40], we also observed that the copper species were oxidized to copper phyllosilicate by the esters during the lifetime test. From this perspective, there is still room for improvement in this Ni/SiO$_2$-AEM.

The above results suggest that the Ni/SiO$_2$-AEM exhibits better performance compared to the Ni/SiO$_2$-IM for CO$_2$ methanation. The preparation method significantly affects their structures and activities. On the basis of the above characterizations, the improved performance of Ni/SiO$_2$-AEM can be attributed to higher surface area, well-dispersed nickel species and silica spheres, smaller average nickel particle sizes, and larger amount of surface acid sites. Furthermore, the catalytic performance of Ni/SiO$_2$-AEM is comparable with other reported Ni−Si or Ni-Metal oxide catalysts
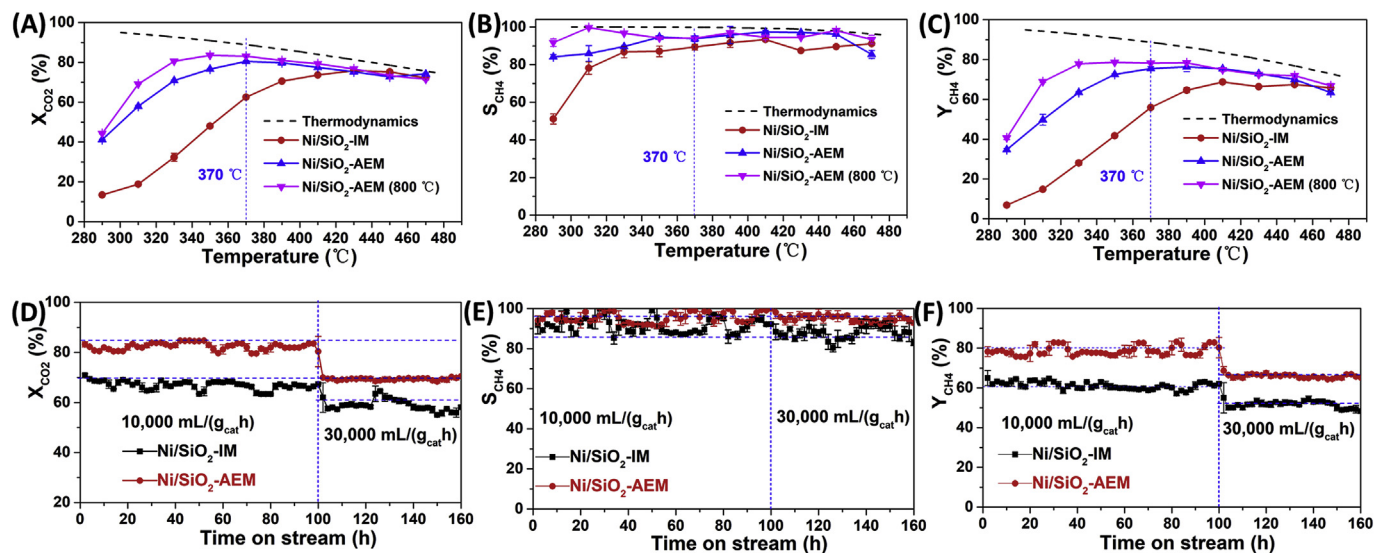
Fig. 9. Catalytic performance of the Ni/SiO$_2$-IM and Ni/SiO$_2$-AEM catalysts reduced at 500 °C, as well as Ni/SiO$_2$-AEM (800 °C) sample reduced at 800 °C. The thermodynamics data was reproduced from reference with acknowledgement [39].

(Table S1).

The in-situ DRIFTS spectra were further used to compare the methanation pathway over the Ni/SiO$_2$ catalysts. Both samples were firstly reduced at 500 °C for 2 h in a tube furnace and *in-situ* reduced at 300 °C for 30 min prior to injecting CO$_2$ gas. As shown in Fig. 10, the hydroxyl groups were observed between 3550 and 3750 cm^{-1} in both Ni/SiO$_2$ samples [41]. The bands at around 3017 and 1305 cm^{-1} suggest the formation of methane from 250 to 350 °C [41]. Compared with Fig. 10A and B, it is worth noting that the bands of carbonate at 1008 and 1282 cm^{-1} were obvious in the Ni/SiO$_2$-IM [42]. However, the Ni/SiO$_2$-AEM displayed obvious bands of formate and absorbed CO on Ni sites at 2850 and 1572 cm^{-1}, 2015 and 1860 cm^{-1}, respectively [43]. Therefore, it

indicates that the Ni/SiO$_2$-AEM exhibits higher activity to convert CO$_2$ to intermediates of formate and CO under the same conditions than the Ni/SiO$_2$-IM.

4. Conclusions

In conclusion, an efficient and stable Ni/SiO$_2$ nanocatalyst without any promoter has been successfully synthesized by an ammonia-evaporation method for CO$_2$ methanation. The significance of this work is summarized in the following paragraphs.

The ammonia-evaporation method was employed to prepare Ni/SiO$_2$ catalyst with unique layered structure and highly dispersed nickel species. The formation of nickel phyllosilicate is beneficial for
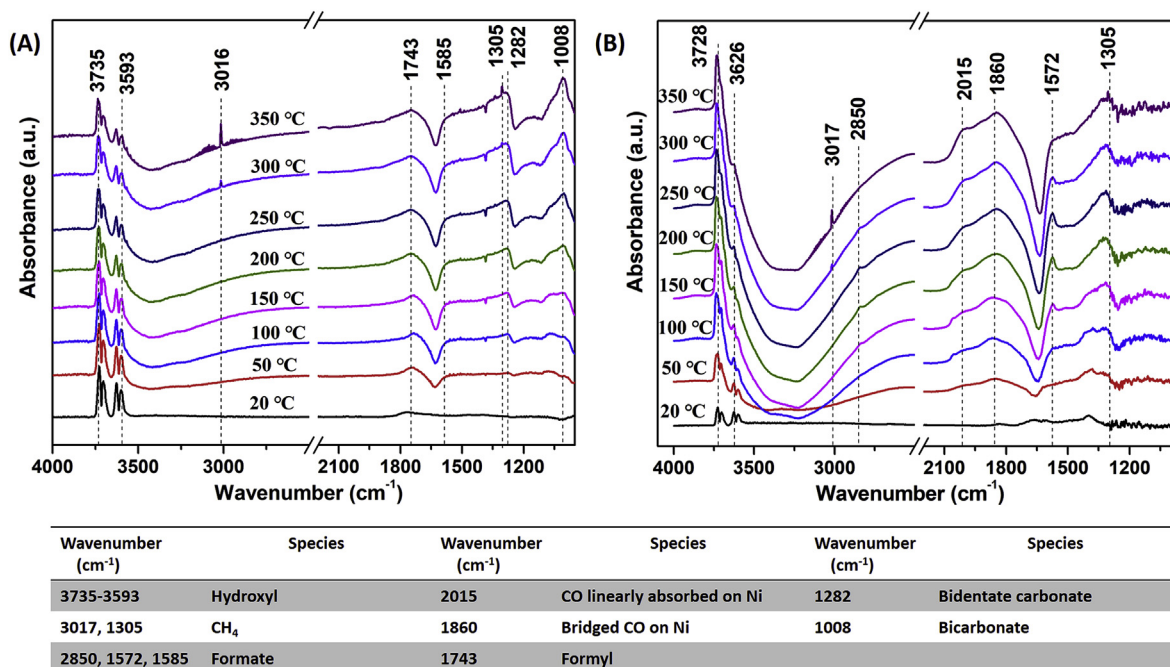

Wavenumber (cm^{-1})	Species	Wavenumber (cm^{-1})	Species	Wavenumber (cm^{-1})	Species
3735-3593	Hydroxyl	2015	CO linearly absorbed on Ni	1282	Bidentate carbonate
3017, 1305	CH$_4$	1860	Bridged CO on Ni	1008	Bicarbonate
2850, 1572, 1585	Formate	1743	Formyl		

Fig. 10. *In-situ* DRIFTS spectra under CO$_2$ methanation conditions over the Ni/SiO$_2$-IM (A) and Ni/SiO$_2$-AEM (B) catalysts.

generating more ultrasmall nickel particles with high dispersion and a strong interaction with the silica support upon reduction. The mean particle size of the Ni/SiO$_2$-AEM is about 4.2 nm, which is much smaller than other Ni-based catalysts prepared by impregnation method. Also, owing to the layered structure of nickel phyllosilicate, the specific surface area of the Ni/SiO$_2$-AEM is as high as 446.3 m^2/g, which is much higher than the catalysts with structures of hydrotalcites or perovskites.

This work indicates that the Ni/SiO$_2$-AEM shows an increased lifetime while exhibiting a high yield of methane than the Ni/SiO$_2$-IM prepared by impregnation method. No deactivation was found in the Ni/SiO$_2$-AEM for 100 h under the GHSV of 10,000 mL/(g$_{cat}$ h) and even 60 h under the GHSV of 30,000 mL/(g$_{cat}$ h) at 370 °C, which is better than most of previously reported Ni/SiO$_2$-IM catalysts that would be deactivated in 20 h. The improved properties of the Ni/SiO$_2$-AEM is owing to its unconventional structure. The catalytic performance including CH$_4$ yield and lifetime of Ni/SiO$_2$-AEM is also comparable with the state-of-the-art Ni−Si or Ni-Metal oxide catalysts prepared by homogeneous precipitation method, wash-coating method, or sol-gel method. Therefore, the ammonia-evaporation method has been illustrated to be an effective and significant approach to prepare Ni−Si based catalysts with high nickel loading and excellent stability. However, some nickel ions would be lost during the preparation process, thus further improvement on the ammonia-evaporation method should be done in future.

Acknowledgements

Appendix A. Supplementary data

Supplementary data to this article can be found online at https://doi.org/10.1016/j.energy.2019.116059.

References

[1] Pandey D, Ray K, Bhardwaj R, Bojja S, Chary KVR, Deo G. Promotion of unsupported nickel catalyst using iron for CO$_2$ methanation. Int J Hydrogen Energy 2018;43:4987−5000.

[2] Veselovskaya JV, Parunin PD, Netskina OV, Kibis LS, Lysikov AI, Okunev AG. Catalytic methanation of carbon dioxide captured from ambient air. Energy 2018;159:766−73.

[3] Yang Y, Liu J, Shen WF, Li J, Chien IL. High-efficiency utilization of CO$_2$ in the methanol production by a novel parallel-series system combining steam and dry methane reforming. Energy 2018;158:820−9.

[4] Li W, Wang H, Jiang X, Zhu J, Liu Z, Guo X, Song C. A short review of recent advances in CO$_2$ hydrogenation to hydrocarbons over heterogeneous catalysts. RSC Adv 2018;8:7651−69.

[5] Liu Q, Tian YY. One-pot synthesis of NiO/SBA-15 monolith catalyst with a three-dimensional framework for CO$_2$ methanation. Int J Hydrogen Energy 2017;42:12295−300.

[6] Guo M, Lu GX. The effect of impregnation strategy on structural characters and CO$_2$ methanation properties over MgO modified Ni/SiO$_2$ catalysts. Catal Commun 2014;54:55−60.

[7] Zhu PF, Chen QJ, Yoneyama Y, Tsubaki N. Nanoparticle modified Ni-based bimodal pore catalysts for enhanced CO$_2$ methanation. RSC Adv 2014;4: 64617−24.

[8] Ren J, Qin X, Yang JZ, Qin ZF, GUo HL, Lin JY, Li Z. Methanation of carbon dioxide over Ni-M/ZrO$_2$ (M=Fe, Co, Cu) catalysts: effect of addition of a second

[9] Mutz B, Belimov M, Wang W, Sprenger P, Serrer MA, Wang D, Pfeifer P, Kleist W, Grunwaldt J-D. Potential of an alumina-supported Ni$_3$Fe catalyst in the methanation of CO$_2$: impact of alloy formation on activity and stability. ACS Catal 2017;7:6802−14.

[10] Mihet M, Lazar MD. Methanation of CO$_2$ on Ni/γ-Al$_2$O$_3$: influence of Pt, Pd or Rh promotion. Catal Today 2018;306:294−9.

[11] Xu LL, Wang FG, Chen MD, Nie DY, Lian XB, Lu ZY, Chen HX, Zhang K, Ge PX. CO$_2$ methanation over rare earth doped Ni based mesoporous catalysts with intensified low-temperature activity. Int J Hydrogen Energy 2017;42: 15523−39.

[12] Su X, Xu JH, Liang BL, Duan HM, Hou BL, Huang YQ. Catalytic carbon dioxide hydrogenation to methane: a review of recent studies. J Energy Chem. 2016;25:553−65.

[13] Chen CS, Budi CS, Wu HC, Saikia D, Kao HM. Size-tunable Ni nanoparticles supported on surface-modified, cage-type mesoporous silica as highly active catalysts for CO$_2$ hydrogenation. ACS Catal 2017;7:8367−81.

[14] Bacariza MC, Graça I, Bebiano SS, Lopes JM, Henriques C. Micro- and mesoporous supports for CO$_2$ methanation catalysts: a comparison between SBA-15, MCM-41 and USY zeolite. Chem Eng Sci 2018;175:72−83.

[15] Liu J, Li CM, Wang F, He S, Chen H, Zhao YF, Wei M, Evans DG, Duan X. Enhanced low-temperature activity of CO$_2$ methanation over highly-dispersed Ni/TiO$_2$ catalyst. Catal. Sci. Technol. 2013;3:2627−33.

[16] Aljishi A, Veilleux G, Hernandez Lalinde JA, Kopyscinski J. The effect of synthesis parameters on ordered mesoporous nickel alumina catalyst for CO$_2$ methanation. Appl Catal Gen 2018;549:263−72.

[17] Solis-Garcia A, Louvier-Hernandez JF, Almendarez-Camarillo A, Fierro-Gonzalez JC. Participation of surface bicarbonate, formate and methoxy species in the carbon dioxide methanation catalyzed by ZrO$_2$-supported Ni. Appl Catal B: Environ 2017;218:611−20.

[18] Atzori L, Cutrufello MG, Meloni D, Cannas C, Gazzoli D, Monaci R, Sinia MF, Rombi E. Highly active NiO-CeO$_2$ catalysts for synthetic natural gas production by CO2 methanation. Catal Today 2018;299:183−92.

[19] Zheng WL, Li B, Lu GX, Ma JT. Enhancing catalytic activity and stability for CO$_2$ methanation on Ni@MOF-5 via control of active species dispersion. Chem Commun 2015;51:1728−31.

[20] Manikandan M, Venugopal AK, Prabu K, Jha RK, Thirumalaiswamy R. Role of surface synergistic effect on the performance of Ni-based hydrotalcite catalyst for highly efficient hydrogenation of furfural. J Mol Catal A Chem 2016;417: 153−62.

[21] Zhou GL, Liu HR, Cui KK, Xie HM, Jiao ZJ, Zhang GZ, Xiong K, Zheng XX. Methanation of carbon dioxide over Ni/CeO$_2$ catalysts: effects of support CeO$_2$ structure. Int J Hydrogen Energy 2017;42:16108−17.

[22] Song FJ, Zhong Q, Yu Y, Shi MG, Wu YH, Hu JH, Song Y. Obtaining well-dispersed Ni/Al$_2$O$_3$ catalyst for CO$_2$ methanation with a microwave-assisted method. Int J Hydrogen Energy 2017;42:4174−83.

[23] Ye RP, Lin L, Yang JX, Sun ML, Li F, Li B, Yao YG. A new low-cost and effective method for enhancing the catalytic performance of Cu−SiO$_2$ catalysts for the synthesis of ethylene glycol via the vapor-phase hydrogenation of dimethyl oxalate by coating the catalysts with dextrin. J Catal 2017;350:122−32.

[24] Qin HY, Guo CL, Sun CW, Zhang JL. Influence of the support composition on the hydrogenation of methyl acetate over Cu/MgO-SiO$_2$ catalysts. J Mol Catal A Chem 2015;409:79−84.

[25] Li FJ, Wang LG, Han X, Cao Y, He P, Li HQ. Selective hydrogenation of ethylene carbonate to methanol and ethylene glycol over Cu/SiO$_2$ catalysts prepared by ammonia evaporation method. Int J Hydrogen Energy 2017;42:2144−56.

[26] Dong F, Ding GQ, Zheng HY, Xiang XM, Chen LF, Zhu YL, Li YW. Highly dispersed Cu nanoparticles as an efficient catalyst for the synthesis of the biofuel 2-methylfuran. Catal Sci Technol 2016;6:767−79.

[27] Wang ZQ, Xu ZN, Peng SY, Zhang MJ, Lu G, Chen QS, Chen YM, Guo GC. High-performance and long-lived Cu/SiO$_2$ nanocatalyst for CO$_2$ hydrogenation. ACS Catal 2015;5:4255−9.

[28] Zhang CX, Yue HL, Huang ZQ, Li SR, Wu GW, Ma XB, Gong JL. Hydrogen production via steam reforming of ethanol on phyllosilicate-derived Ni/SiO2: enhanced metal-support interaction and catalytic stability. ACS Sustain Chem Eng 2013;1:161−73.

[29] Zhang QL, Wang MZ, Zhang TF, Wang YR, Tang XS, Ning P. A stable Ni/SBA-15 catalyst prepared by the ammonia evaporation method for dry reforming of methane. RSC Adv 2015;5:94016−24.

[30] Yang FF, Wang H, Han JY, Ge QF, Zhu XL. Enhanced selective deoxygenation of m-cresol to toluene on Ni/SiO$_2$ catalysts derived from nickel phyllosilicate. Catal Today 2019;330:149−56.

[31] Kong X, Zhu YF, Zheng HY, Li XQ, Zhu YL, Li YW. Ni nanoparticles inlaid nickel phyllosilicate as a metal−acid bifunctional catalyst for low-temperature hydrogenolysis reactions. ACS Catal 2015;5:5914−20.

[32] Li CS, Zhu XF, Le Y, Zhu BC, Yu JG, Ho WK. Hierarchically porous NiO-Al$_2$O$_3$ nanocomposite with enhanced Congo red adsorption in water. RSC Adv 2016;6:10272−9.

[33] Li Q, Liang CL, Lu XF, Tong YX, Li GR. Ni@NiO core−shell nanoparticle tube arrays with enhanced supercapacitor performance. J Mater Chem A 2015;3: 6432−9.

[34] Chen LF, Guo PJ, Qiao MH, Yan SR, Li HX, Shen W, Xu HL, Fan KN. Cu/SiO$_2$ catalysts prepared by the ammonia-evaporation method: texture, structure, and catalytic performance in hydrogenation of dimethyl oxalate to ethylene glycol. J Catal 2008;257:172−80.

[35] Sivaiah MV, Petit S, Barrault J, Batiot-Dupeyrat C, Valange S. CO_2 reforming of CH_4 over Ni-containing phyllosilicates as catalyst precursors. Catal Today 2010;157:397−403.

[36] Bian ZF, Kawi S. Sandwich-like silica@Ni@Silica multicore-shell catalyst for the low-temperature dry reforming of methane: confinement effect against carbon formation. ChemCatChem 2018;10:320−8.

[37] Yang MH, Jin P, Fan YR, Huang CJ, Zhang NW, Weng WZ, Chen MS, Wan HL. Ammonia-assisted synthesis towards a phyllosilicate-derived highly-dispersed and long-lived Ni/SiO_2 catalyst. Catal. Sci. Technol. 2015;5:5095−9.

[38] Zhao BR, Chen ZP, Chen YJ, Ma XJ. Syngas methanation over Ni/SiO_2 catalyst prepared by ammonia-assisted impregation. Int J Hydrogen Energy 2017;42: 27073−83.

[39] Gao JJ, Wang YL, Ping Y, Hu DC, Xu GW, Gu GW, Su FB. A thermodynamic analysis of methanation reactions of carbon oxides for the production of synthetic natural gas. RSC Adv 2012;2:2358−68.

[40] Ye RP, Lin L, Liu CQ, Chen CC, Yao YG. One-pot synthesis of cyclodextrin doped $Cu-SiO_2$ catalysts for efficient hydrogenation of dimethyl oxalate to ethylene glycol. ChemCatChem 2017;9:4587−97.

[41] Ashok J, Ang ML, Kawi S. Enhanced activity of CO_2 methanation over Ni/CeO_2-ZrO_2 catalysts: influence of preparation methods. Catal Today 2017;281: 304−11.

[42] Zhou GL, Liu HR, Cui KK, Jia AP, Hu GS, Jiao ZJ, Liu YQ, Zhang XM. Role of surface Ni and Ce species of Ni/CeO_2 catalyst in CO_2 methanation. Appl Surf Sci 2016;383:248−52.

[43] Guo Y, Mei S, Yuan K, Wang DJ, Liu HC, Yan CH, Zhang YW. Low-temperature CO_2 methanation over CeO_2-supported Ru single atoms, nanoclusters, and nanoparticles competitively tuned by strong metal−support interactions and H-spillover effect. ACS Catal 2018;8:6203−15.